Pergamon

Int. J. Heat Mass Transfer. Vol. 38, No. 16, pp. 3077–3084, 1995

0017-9310/95 $9.50+0.00

0017-9310(95)00008-9

Numerical analysis of deterioration phenomena in heat transfer to supercritical water

S. KOSHIZUKA, N. TAKANO and Y. OKA

Nuclear Engineering Research Laboratory, Faculty of Engineering, The University of Tokyo, 2-22 Shirane, Shirakata, Tokai-mura, Naka-gun, Ibaraki 319-11, Japan

(*Received* 8 *July* 1994 *and in final form* 1 *December* 1994)

Abstract—Deterioration in heat transfer at supercritical water cooling in a vertical pipe is numerically analyzed. The calculation is based on a parabolic solver for steady-state equations in r–z two dimensions, a k–ε model for turbulence and a steam table library for physical properties of supercritical water. Calculation results agree with the experimental data of Yamagata *et al.* It is found that heat transfer deterioration is caused by two mechanisms depending on the flow rate. When the heat flux is increased much above the deterioration heat flux, a violent oscillation is observed in the temperature distribution.

1. INTRODUCTION

At supercritical pressure, the boundary between liquid and gas phases disappears. Density continuously decreases when temperature increases as Fig. 1. Specific heat shows a peak at pseudo-critical temperature where the density change is maximum. It has been known that supercritical fluids exhibit unusual phenomena near the pseudo-critical temperature. The heat transfer coefficient is enhanced when the heat flux is low, while it is deteriorated or oscillated when the heat flux is high [1–9]. Correlations of the heat transfer coefficient and criteria of the deterioration have been developed on the basis of experiments. These correlations and criteria are used, for example, in the design of supercritical pressure fossil fired plants. The authors have been studying the design of nuclear reactors cooled by supercritical water for improving the efficiency of power generation and to simplify the plant system [10–14]. However the correlations which were obtained by the specific experiments are not available when the flow conditions are much changed ; a flow channel is surrounded by a triangular array of pipes in the designed reactors.

The unusual phenomena of supercritical fluids have been explained by many theories, which are roughly categorized into two types : single-phase and two-phase fluid dynamics. However the conclusion has not been obtained yet. In the theory based on single-phase fluid dynamics, unusual behaviors are attributed to single-phase turbulent flow with excessive change of physical properties by heating. On the other hand, pseudo-boiling is assumed in the theory based on two-phase fluid dynamics. Deterioration of heat transfer is explained by transition from pseudo-nucleate to pseudo-film boiling.

Analytical studies assuming the single-phase fluid dynamics have been carried out [2, 5, 15, 16]. In these studies mixing length models were employed for turbulence. Since this type of model requires the distribution of turbulent viscosity in advance, a special assumption is used to incorporate effect of excessive change of physical properties. In this case, validity of the special assumption remains for discussion even if the calculation result agrees with the experimental one. In addition, change of density is not considered in the continuity and momentum equations, which implies that buoyancy force and fluid expansion are not incorporated. Therefore these studies were applicable to limited flow conditions.

The present calculations are based on a k–ε model by Jones-Launder [17]. It has a more general description for turbulence than the mixing length models. Effects of buoyancy force and fluid expansion on the heat transfer to normal fluids have been successfully analyzed by the k–ε model [17, 18]. Physical properties are treated as variables in the governing equations and evaluated from a steam table library [19]. Thus extremely nonlinear physical properties of supercritical water are evaluated directly and correctly. The present approach is applicable to wide range of flow

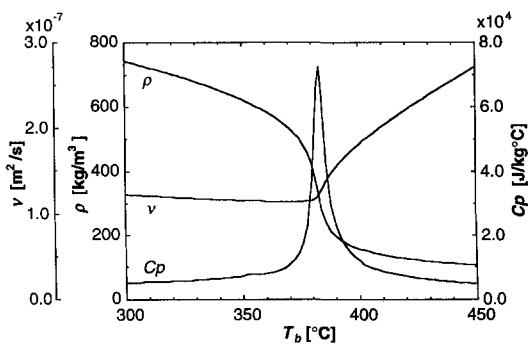

Fig. 1. Physical properties of supercritical water near the pseudo-critical temperature $T_m = 383°C$ at $P = 2.452 \times 10^7$Pa.

NOMENCLATURE

C_p specific heat
c_μ, c_1, c_2 constants in the k–ε model
d pipe inner diameter
f_μ, f_1, f_2 functions in the k–ε model
G flow rate
Gr Grashof number ; $g[(\rho_b-\rho_f)/\rho_b][d^3/\nu_f^2]$
g gravitational constant
H enthalpy
h pipe height
k turbulence kinetic energy
Nu Nusselt number, $\alpha d/\lambda_f$
P pressure
Pr Prandtl number, $\rho C_p \nu/\lambda$
Pr_t turbulent Prandtl number
q'' heat flux
Re Reynolds number, $U_b d/\nu_b$
R_t turbulent Reynolds number, $k^2/\nu\varepsilon$
r radial coordinate
T temperature
U axial velocity component
V radial velocity component
y normal distance from the wall
z axial coordinate.

Greek symbols
α heat transfer coefficient, $q''/(T_w-T_b)$
α_0 ideal heat transfer coefficient at $q''=0$
ε dissipation rate of turbulence kinetic energy
λ thermal conductivity
ν kinematic viscosity
ν_t kinematic viscosity of turbulence
ρ density
σ_k, σ_ε constants in the k–ε model.

Subscripts
b bulk
f film, $1/2\ (T_w+T_b)$
m pseudo-critical point
w inner wall surface.

conditions of supercritical water without any special assumption.

In Section 2, numerical methods are described. The calculation results are compared with the experimental ones by Yamagata *et al.* [6] in Section 3. Mechanisms of the deterioration are considered in Section 4. An oscillation of the inner wall temperature distribution is presented and discussed in Section 5. Conclusions are noted in Section 6.

2. CALCULATION MODELS

2.1. *Governing equations*

Governing equations are the continuity equation, the Navier–Stokes equations and transport equations of k, ε and enthalpy in r–z two dimensions. The Jones–Launder's k–ε model is employed for turbulence [17]. To use a parabolic solver, diffusion terms in the z-direction and pressure profile in the r-direction are neglected. Since vertical variation of density is much smaller than radial one in the pipe geometry that is analyzed in this study, an additional generation term of turbulence derived from the buoyancy force is neglected.

$$\frac{\partial}{\partial z}(\rho U)+\frac{1}{r}\frac{\partial}{\partial r}(r\rho V)=0 \tag{1}$$

$$\frac{\partial}{\partial z}(\rho UU)+\frac{1}{r}\frac{\partial}{\partial r}(r\rho VU)=-\frac{\partial P}{\partial z}+\frac{1}{r}\frac{\partial}{\partial r}\left[\rho(\nu+\nu_t)r\frac{\partial U}{\partial r}\right]-\rho g \tag{2}$$

$$\nu_t=c_\mu f_\mu\frac{k^2}{\varepsilon} \tag{3}$$

$$\frac{\partial}{\partial z}(\rho Uk)+\frac{1}{r}\frac{\partial}{\partial r}(r\rho Vk)=\frac{1}{r}\frac{\partial}{\partial r}\left[\rho\left(\nu+\frac{\nu_t}{\sigma_k}\right)r\frac{\partial k}{\partial r}\right]+\rho\nu_t\left(\frac{\partial U}{\partial r}\right)^2-\rho\varepsilon-2\rho\nu\left(\frac{\partial k^{1/2}}{\partial r}\right)^2 \tag{4}$$

$$\frac{\partial}{\partial z}(\rho U\varepsilon)+\frac{1}{r}\frac{\partial}{\partial r}(r\rho V\varepsilon)=\frac{1}{r}\frac{\partial}{\partial r}\left[\rho\left(\nu+\frac{\nu_t}{\sigma_\varepsilon}\right)r\frac{\partial\varepsilon}{\partial r}\right]+c_1f_1\frac{\varepsilon}{k}\rho\nu_t\left(\frac{\partial U}{\partial r}\right)^2-c_2f_2\rho\frac{\varepsilon^2}{k}+2\rho\nu\nu_t\left(\frac{\partial^2U}{\partial r^2}\right)^2 \tag{5}$$

where

$$f_\mu=\exp\left(\frac{-2.5}{1+R_t/50}\right)\quad f_1=1.0$$

$$f_2=1.0-0.3\exp(-R_t^2),\quad R_t=k^2/\nu\varepsilon.$$

Constants in the turbulence model are represented in Table 1. The transport equation of enthalpy is

Table 1. Values of the constants in the k–ε model

c_μ	c_1	c_2	σ_k	σ_ε
0.09	1.45	2.0	1.0	1.3

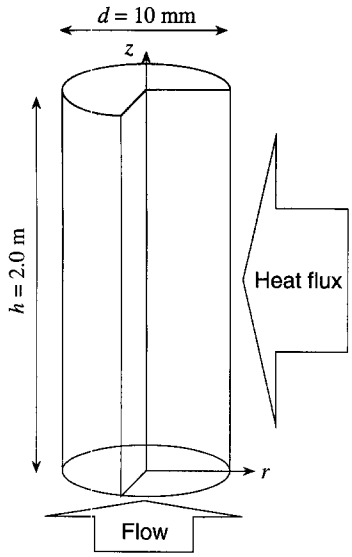

Fig. 2. Calculation geometry.

$$\frac{\partial}{\partial z}(\rho UH)+\frac{1}{r}\frac{\partial}{\partial r}(r\rho VH) = \frac{1}{r}\frac{\partial}{\partial r}\left[\rho C_p\left(\frac{\nu}{Pr}+\frac{\nu_t}{Pr_t}\right)r\frac{\partial T}{\partial r}\right] \quad (6)$$

where Pr_t is the turbulent Prandtl number and is set constant 0.9. The fluid is water and its physical properties are calculated from a steam table library [19].

2.2. *Numerical methods*

The solution algorithm is based on the parabolic solver of Patankar–Spalding [20]. The steady-state solution is obtained by marching from the inlet to the outlet in the z-direction. At each position of z, an implicit calculation is performed by an iterative method and a radial distribution of axial flow velocities is obtained. The physical properties are updated in each iteration. The pressure value, which is constant in the radial direction, is determined to keep the total axial flow rate. The radial flow velocities are calculated from the continuity equation.

The calculation geometry is a vertical pipe with height 2 m and inner diameter 1.0 cm as shown in Fig. 2. The wall surface is heated uniformly. Water flows into the pipe at the bottom. The inlet velocity profile is given as that of the fully developed turbulent flow, which is obtained by a preliminary calculation with constant physical properties of the inlet temperature. The inlet temperature profile is set uniform. A constant pressure is used for the physical properties.

Non-uniform grids are employed. In the r-direction, the mesh adjacent to the wall has the minimum width, which is determined such that the non-dimensional length y^+ is lower than 0.1 at the largest Reynolds number (approximately 420,000 in the present analysis). The mesh width is enlarged by 1.2 toward the center of the pipe till it reaches the maximum limit 1.0×10^{-4} m. The mesh width is kept constant at this limit near the center. Consequently, the radial mesh size was 83. In the z-direction, the mesh width is controlled to avoid numerical oscillations. Alternate increase and decrease of temperature appear when this type of oscillations occurs. Particularly, the mesh width should be finer near the inlet boundary where the radial temperature distribution, which is set uniform at the inlet, rapidly changes. The mesh size should be finer for higher heat flux, smaller mass flow rate or higher enthalpy as well. Therefore the mesh sizes in z-direction are greatly different in the cases.

Results of fully developed turbulent flow with constant physical properties agreed well with those presented in ref. [21].

3. NUMERICAL RESULTS

3.1. *Effect of the heat flux*

Calculations were carried out with three values of the heat flux, 2.33, 4.65 and 9.30×10^5 W m^{-2}, at 2.452×10^7 Pa. Since the inlet temperature profile is set uniform, the wall surface temperature is low and the heat transfer coefficient is high near the inlet boundary. Thus this developing region is removed from the calculation results. Many cases of different inlet temperatures are calculated and relation between the heat transfer coefficient and the bulk enthalpy is obtained in wide range. Comparison is made with the experimental data by Yamagata *et al.* [6] in Fig. 3. The heat transfer coefficient shows a maximum peak near the pseudo-critical temperature. The peak decreases and moves to the lower bulk enthalpy as the

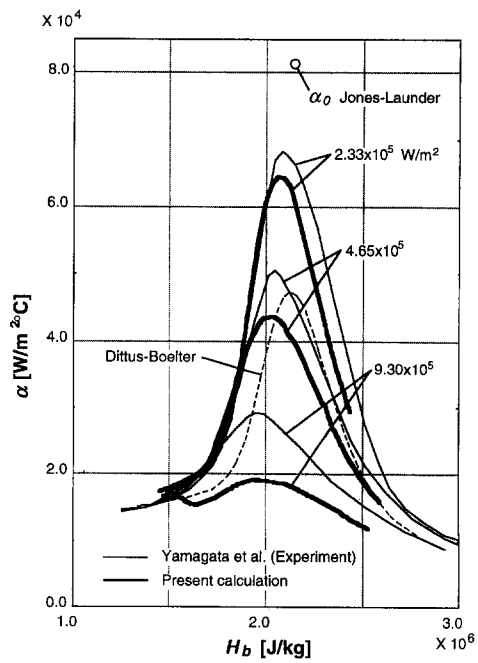

Fig. 3. Heat transfer coefficient near the pseudo-critical temperature ; comparison with the experimental data of Yamagata *et al.* [6] and Dittus–Boelter's correlation.

heat flux increases. These behaviors agree with the experimental data.

The present results show better agreement than those of the mixing length model in [16]. This is mainly attributed to the formulation of extreme change of physical properties in the governing equations. In the present analysis, change of physical properties affects many terms in the governing equations, while most of them are neglected or approximated when the mixing length model is used.

Heat transfer coefficients calculated by the Dittus–Boelter's correlation,

$$Nu = 0.023 Re_b^{0.8} Pr_b^{0.4} \quad (7)$$

are drawn in Fig. 3 as well. The Dittus–Boelter's correlation gives the ideal coefficient α_0 at the heat flux being zero because constant physical properties at the bulk temperature are assumed in it. Though the Dittus–Boelter's correlation gives smaller coefficients than those at the smallest heat flux, 2.33×10^5 W m^{-2}, we should not conclude that the heat transfer coefficient is enhanced at low heat fluxes. It is known that the Dittus–Boelter's correlation shows relatively small heat transfer coefficients at high Prandtl numbers. Thus the coefficient near the pseudo-critical temperature, where the Prandtl number becomes large, can be smaller. The ideal coefficient calculated by the Jones–Launder's k–ε model at the pseudo-critical temperature is plotted in Fig. 3. It is calculated by fixing the physical properties at the pseudo-critical temperature. This value is higher than the curve of 2.33×10^5 W m^{-2}. When the Jones–Launder k–ε model is used, it is known that the wall shear stress is relatively large, and that the heat transfer coefficient is also large with a constant turbulent Prandtl number. As indicated by Jackson and Hall [8], the heat transfer coefficient is maximum at the heat flux being zero and it monotonically decreases as the heat flux increases. The present analysis supports their assertion.

3.2. *Deterioration heat flux*

To obtain the deterioration heat flux, calculations were carried out with various combinations of the flow rate G and the heat flux q''. Deterioration is assessed where the bulk temperature reaches the pseudo-critical temperature. Deterioration ratio α/α_0 is defined where α_0 is the ideal heat transfer coefficient mentioned above. The calculation results are shown in Fig. 4. The heat transfer coefficient monotonically decreases when the flow rate is large. On the other hand, it abruptly drops at a certain heat flux and maintains a constant value or increases with larger heat fluxes when the flow rate is small. The boundary is around 200 kg m^{-2} s^{-1} in the present flow conditions. These behaviors suggest that there exist different mechanisms of deterioration depending on the flow rate.

A map of deterioration is presented in Fig. 5. Occurrence of deterioration is judged when the deterioration

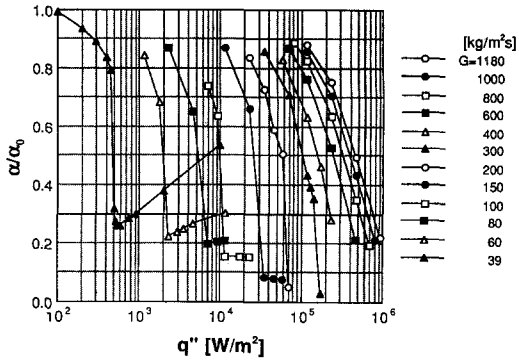

Fig. 4. Heat transfer deterioration of various flow rates ; α : heat transfer coefficient ; α_0 : ideal heat transfer coefficient at $q'' = 0$.

ratio is smaller than 0.3 in the present analysis. The correlation by Yamagata *et al.* is also provided in Fig. 5. This correlation was obtained where the heat transfer coefficient was deteriorated to $\frac{1}{2}$–$\frac{2}{3}$ compared with that of normal heat transfer predicted by their own formula. The present calculation results agree with the correlation by Yamagata *et al.* when the flow rate is high. The slope of the curve becomes steep when the flow rate is small. Deterioration occurs at a relatively small heat flux in this region. There is an arbitrary choice in the present criterion of deterioration, $\alpha/\alpha_0 < 0.3$, but the above discussion will not be much affected by changing this.

4. CONSIDERATION OF HEAT TRANSFER DETERIORATION

4.1. *Heat transfer deterioration at high flow rates*

Radial profiles of flow velocity, turbulence energy, temperature, viscosity and the Prandtl number near the wall ($y = 0 \sim 2.0 \times 10^{-5}$ m) at $G = 1180$ kg m^{-2} s^{-1} and $T_b = T_m$ are shown in Fig. 6. When the heat flux increases, the flow velocity and the turbulence energy decrease near the wall. The viscosity increases

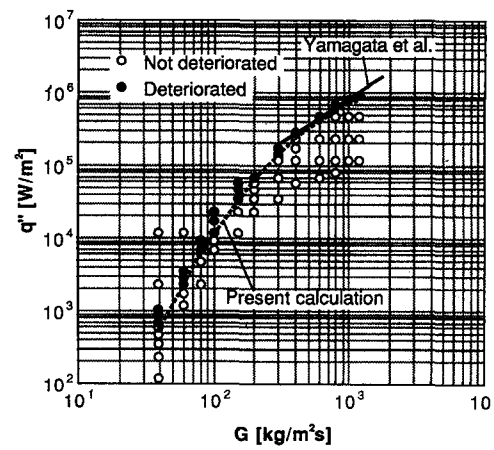

Fig. 5. Map of heat transfer deterioration ; comparison with the correlation by Yamagata *et al.* [6]

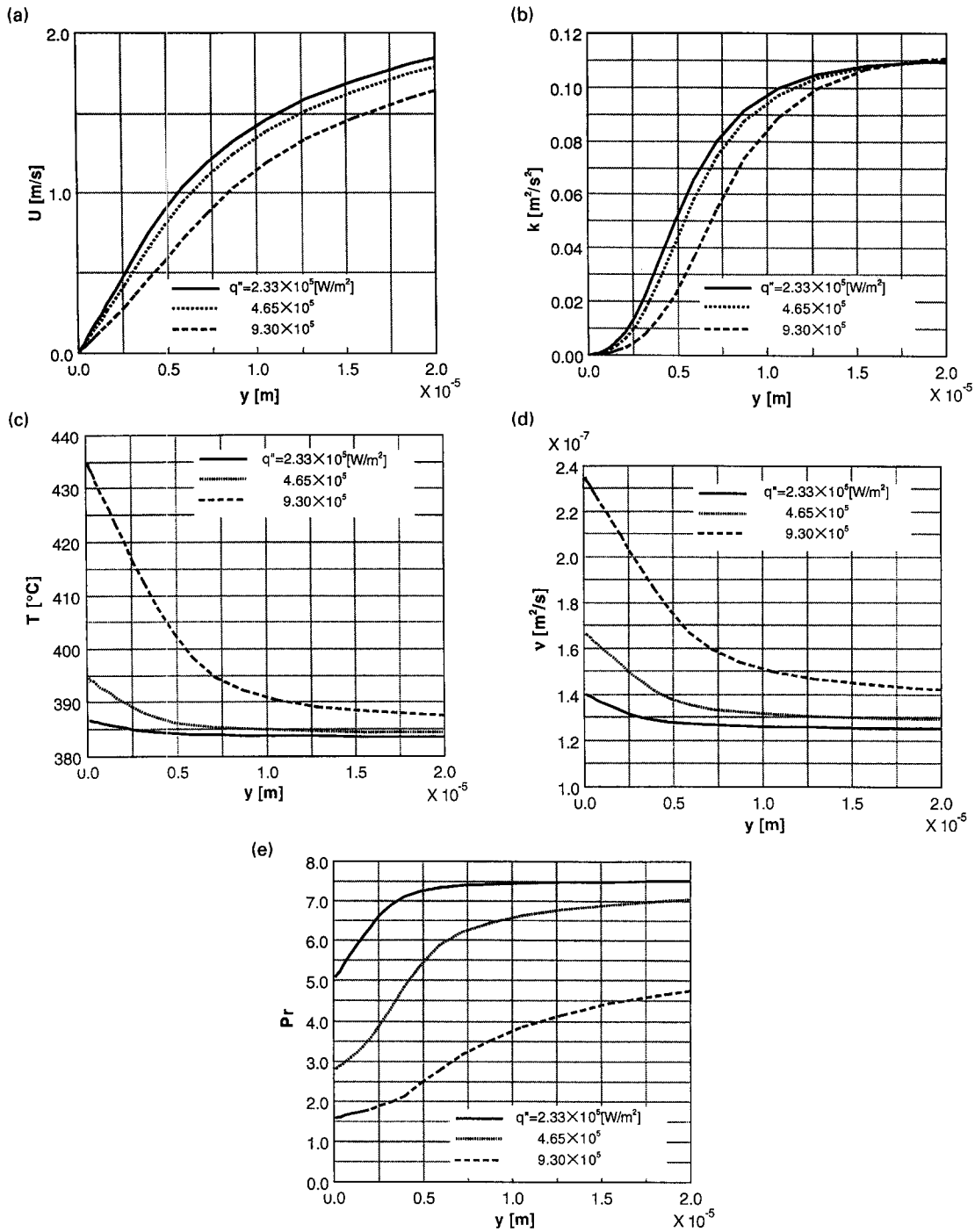

Fig. 6. Radial distributions near the wall at $G = 1180$ kg m^{-2}s^{-1} : (a) flow velocity, (b) turbulence energy, (c) temperature, (d) viscosity and (e) Prandtl number.

and the Prandtl number decreases locally because the temperature is enhanced by heating. Higher viscosity leads to a thicker viscous sublayer, which reduces turbulence near the wall and heat transfer is deteriorated. Smaller Prandtl numbers reduce the heat transfer as well. This explanation is consistent with the monotonic behavior of deterioration at high flow rates.

4.2. *Heat transfer deterioration at low flow rates*

Figures 4 and 5 suggest that deterioration is caused by a different mechanism at low flow rates. The calculation results at $G = 39$ kg m^{-2} s^{-1} and $T_b = T_m$, which gives the Reynolds number 10 000, are rearranged in terms of the Grashof number and the Nusselt number in Fig. 7. The Grashof number, the

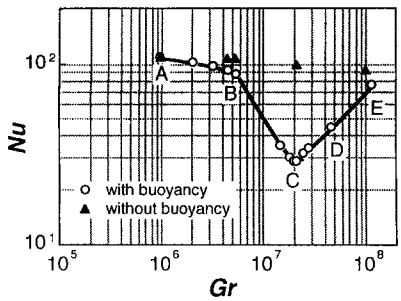

Fig. 7. Relation between Gr and Nu at $G = 39$ kg m^{-2}s^{-1} ; A, 100 ; B, 450 ; C, 550 ; D, 2000 ; E, 10000 W m^{-2}.

Nusselt number and the Reynolds number are defined as

$$Gr = g\frac{(\rho_b - \rho_f)}{\rho_b}\frac{d^3}{\nu_f^2} \tag{8}$$

$$Nu = \frac{q''}{T_w - T_b}\frac{d}{\lambda_f} \tag{9}$$

$$Re = \frac{U_b D}{\nu_b} \tag{10}$$

where subscripts b and w denote bulk and wall, respectively. Subscript f means the film temperature which is the average of bulk and wall temperatures : $T_f = \frac{1}{2}(T_b + T_w)$. As shown in Fig. 7, Nu exhibits a minimum value at $Gr = 2 \times 10^7$. Nu keeps constant when Gr is lower than it, which means that forced convection is dominant. On the other hand, Nu increases linearly when Gr is larger than the minimum point, which implies that natural convection is dominant. The minimum point emerges at the boundary between the two convection modes.

Flow velocity and turbulence energy profiles are depicted in Fig. 8. When the heat flux is enhanced, the flow velocity increases near the wall and the profile becomes flat. Since turbulence energy is produced by the derivative of flow velocity, turbulence energy is reduced. Thus heat transfer is deteriorated. When the heat flux is enhanced more above the minimum point, the flow velocity profile is more distorted and turbulent heat transfer is then enhanced.

It is known that this type of heat transfer deterioration occurs due to acceleration as well as buoyancy. In the present analysis, buoyancy force is dominant. To verify this, calculations were performed without the buoyancy force term in the Navier–Stokes equations. The results are also provided in Fig. 7. Without the buoyancy force term, the minimum point completely disappears.

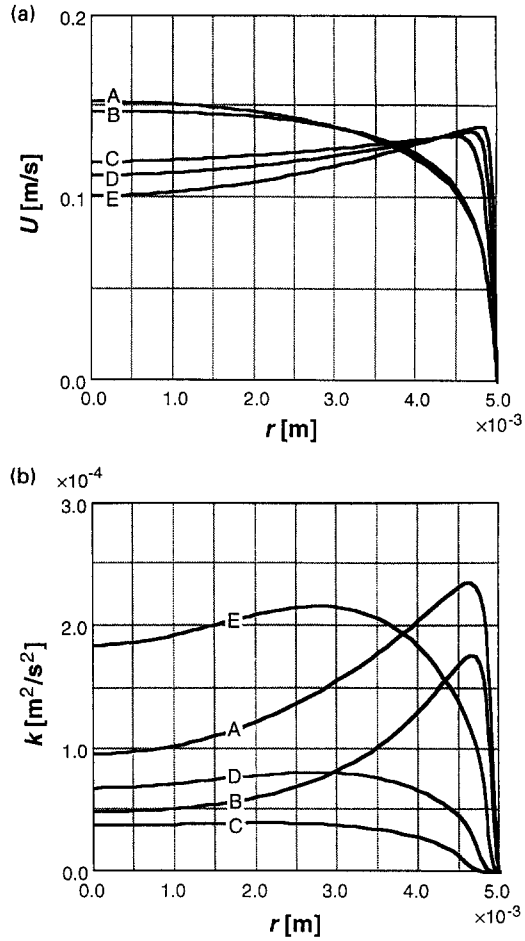

Fig. 8. Radial distributions at $G = 39$ kg m^{-2}s^{-1} ; A, 100 ; B, 450 ; C, 550 ; D, 2000 ; E, 10 000 W m^{-2} : (a) flow velocity and (b) turbulence energy.

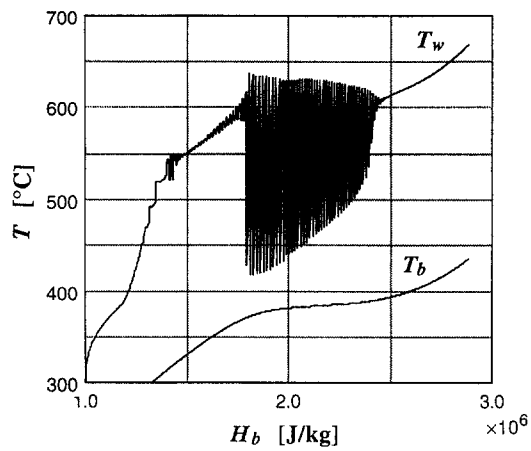

Fig. 9. An oscillation profile of wall temperature at $G = 1180$ kg m^{-2}s^{-1} and $q'' = 1.63 \times 10^6$ W m^{-2}.

5. OSCILLATION OF WALL TEMPERATURE

When the heat flux was enhanced above the critical value of deterioration, a violent oscillation of the wall temperature was observed. Figure 9 shows the axial profile of wall temperature at $G = 1180$ kg m^2 s^{-1} and $q'' = 1.63 \times 10^6$ W m^{-2}. This oscillation is steady-state. An enlarged profile near $H_b = 2.0 \times 10^6$ J kg^{-1} is shown in Fig. 10. The wall temperature gradually increases and abruptly decreases in each cycle. There-

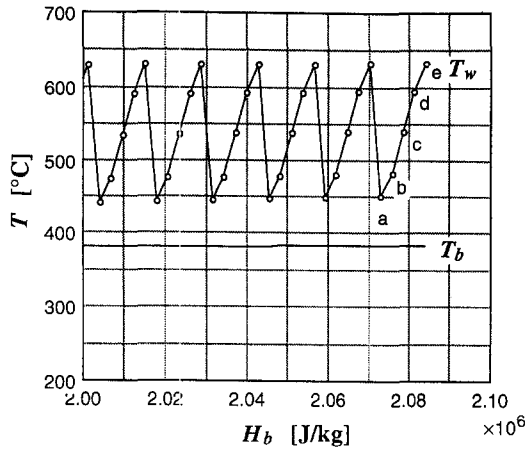

Fig. 10. Transition of wall temperature in the oscillation region ; a, $z = 1.9775$; b, $z = 1.9825$; c, $z = 1.9875$; d, $z = 1.9925$; e, $z = 1.9975$ m.

fore this oscillation is not derived from numerical instability which makes alternate profiles.

Flow velocity, turbulence energy and temperature distributions near the wall are depicted in Fig. 11. When the wall temperature is low (curve a), the viscous sublayer is thin and turbulence energy near the wall is large. As the position moves to the downstream, the viscous sublayer becomes thicker and turbulence energy becomes smaller. Smaller turbulence energy reduces heat transfer, which causes higher temperature. Higher temperature leads to higher viscosity. Higher viscosity leads to a thicker viscous sublayer which further reduces turbulence energy. Therefore a series of these processes has a positive feedback. The boundary layer of temperature becomes several times thicker in a short distance from point a to e. In Fig. 11(c), we can see that temperature difference reaches 200°C in the boundary layer which is only 2×10^{-5} m thick at point e. The inner wall is filmed with very hot water of low density, while cold water of high density remains in the bulk of the pipe. This bulk water is near the pseudo-critical temperature. When mixing is enhanced a little in the steep boundary layer of temperature, for example because of the numerical error, the temperature and the viscosity decrease toward those of the bulk water. This enhances turbulence energy and the mixing in the boundary layer is further promoted. Therefore the steep boundary layer of temperature is suddenly collapsed and returns to being thin. In other words, the steep boundary layer of temperature is unstable when the physical properties nonlinearly change with temperature as those of supercritical water.

Thermo-acoustic oscillations of supercritical fluids were found in experiments and reported [4, 7, 8]. This type of oscillation was explained by the nucleate boiling [4]. The oscillations, however, occur when the heat flux is much enhanced [7], which means that film boiling is changed to nucleate boiling at the critical heat flux. However the nucleate boiling is changed to the film boiling in subcritical fluids. Similarity with the nucleate boiling is unsatisfactory for explaining this.

The present analysis suggests that unstable characteristics of the thick boundary layer of temperature cause the onset of thermo-acoustic oscillations. This is consistent with the experimental result that oscillations occur when the heat flux is much enhanced.

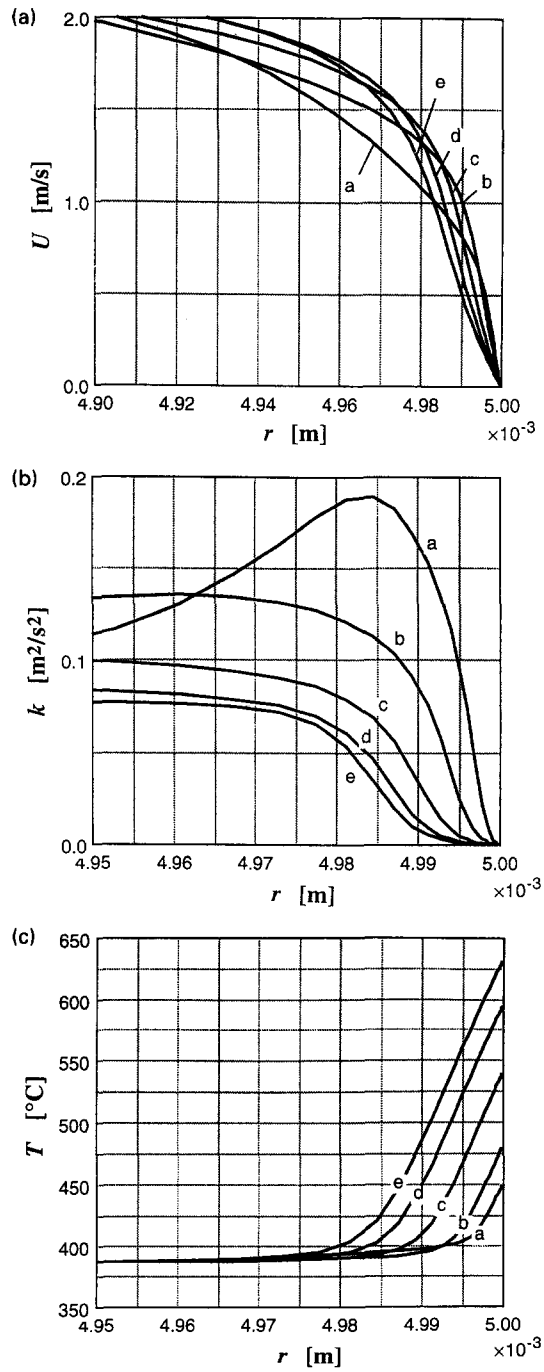

Fig. 11. Radial distributions near the wall at $G = 1180$ kg m^{-2} s^{-1} and $q'' = 1.63 \times 10^6$ W m^{-2}, a, $z = 1.9775$; b, $z = 1.9825$; c, $z = 1.9875$; d, $z = 1.9925$; e, $z = 1.9975$ m : (a) flow velocity, (b) turbulence energy and (c) temperature.

There are many sources of disturbance in the experiments, e.g. inlet boundary conditions or resonance with pipe vibration. In reality, the wall temperature will be oscillated in both space and time as long as the boundary layer of temperature is unstable.

6. CONCLUSIONS

Numerical analysis of heat transfer to supercritical water was carried out. The heat transfer coefficient and the deterioration heat flux calculated in the present analysis agree well with the experimental data by Yamagata *et al.* Heat transfer deterioration occurs due to two mechanisms depending on the flow rate. When the flow rate is large, viscosity increases locally near the wall by heating. This makes the viscous sublayer thicker and the Prandtl number smaller. Both effects reduce the heat transfer. When the flow rate is small, buoyancy force accelerates the flow velocity near the wall. This makes the flow velocity distribution to be flat and generation of turbulence energy is reduced. This type of heat transfer deterioration appears at the boundary between forced and natural convection. As the heat flux increases above the deterioration heat flux, a violent oscillation of wall temperature is observed. It is explained by the unstable characteristics of the steep boundary layer of temperature. Consequently numerical analysis with a k–ε turbulence model and accurate treatment of physical properties leads to successful explanations of unusual heat transfer phenomena of supercritical water.

REFERENCES

1. H. S. Swenson, J. R. Carver and C. R. Kakarala, Heat transfer to supercritical water in smooth-bore tubes, *J. Heat Transfer* **87,** 477–484 (1965).
2. B. S. Shiralkar and P. Griffith, Deterioration in heat transfer to fluids at supercritical pressure and high heat fluxes, *J. Heat Transfer* **91,** 27–36 (1969).
3. B. S. Shiralkar and P. Griffith, The effect of swirl, inlet conditions, flow direction and tube diameter on the heat transfer to fluids at supercritical pressure, *J. Heat Transfer* **92,** 465–474 (1970).
4. J. W. Ackerman, Pseudoboiling heat transfer to supercritical pressure water in smooth and ribbed tubes, *J. Heat Transfer* **92,** 490–498 (1970).
5. H. Tanaka, N. Nishiwaki, M. Hirata and A. Tsuge, Forced convection heat transfer to fluid near critical point flowing in circular tube, *Int. J. Heat Mass Transfer* **14,** 739–750 (1971).
6. K. Yamagata, K. Nishikawa, S. Hasegawa, T. Fujii and S. Yoshida, Forced convection heat transfer to supercritical water flowing in tubes, *Int. J. Heat Mass Transfer* **15,** 2575–2593 (1972).
7. E. Stewart, P. Stewart and A. Watson, Thermo-acoustic oscillations in forced convection heat transfer to supercritical pressure water, *Int. J. Heat Mass Transfer* **16,** 257–270 (1973).
8. J. D. Jackson and W. B. Hall, Forced convection heat transfer to fluids at supercritical pressure. In *Turbulent Forced Convection in Channels and Bundles*, Vol. 2, pp. 563–611. Hemisphere, New York (1979).
9. J. D. Jackson and W. B. Hall, Influences of buoyancy on heat transfer to fluids flowing in vertical tubes under turbulent conditions. In *Turbulent Forced Convection in Channels and Bundles*, Vol. 2, pp. 613–640. Hemisphere, New York (1979).
10. Y. Oka, S. Koshizuka and T. Yamasaki, Direct cycle light water reactor operating at supercritical pressure, *J. Nucl. Sci. Technol.* **29,** 585–588 (1992).
11. T. Jevremovic, Y. Oka and S. Koshizuka, Conceptual design of an indirect-cycle, supercritical steam cooled fast breeder reactor with negative coolant void reactivity characteristics, *Ann. Nucl. Energy* **20,** 305–313 (1993).
12. T. Jevremovic, Y. Oka and S. Koshizuka, Design of an indirect-cycle fast breeder reactor cooled by supercritical steam, *Nucl. Eng. Design* **114,** 337–344 (1993).
13. Y. Oka and S. Koshizuka, Concept and design of a supercritical-pressure, direct-cycle light water reactor, *Nucl. Technol.* **103,** 295–302 (1993).
14. Y. Oka, T. Jevremovic and S. Koshizuka, A direct-cycle, supercritical water-cooled fast breeder reactor, *J. Nucl. Sci. Technol.* **31,** 83–85 (1994).
15. N. M. Schnurr, V. S. Sastry and A. B. Shapiro, A numerical analysis of heat transfer to fluids near the thermodynamic critical point including the thermal entrance region, *J. Heat Transfer* **98,** 609–615 (1976).
16. S. Yoshida, T. Fujii and K. Nishikawa, Analysis of turbulent forced convection heat transfer to a supercritical fluid flowing in a tube, *Trans. Japan Soc. Mech. Engng* **38**(2), 3185–3192 (1972) (in Japanese).
17. W. P. Jones and B. E. Launder, The calculation of low-Reynolds-number phenomena with a two-equation model of turbulence, *Int. J. Heat Mass Transfer* **16,** 1193–1130 (1973).
18. H. Tanaka, S. Maruyama and S. Hatano, Combined forced and natural convection heat transfer for upward flow in a uniformly heated vertical pipe, *Int. J. Heat Mass Transfer* **30,** 165–174 (1987).
19. *Centre News*, Computer Centre of the University of Tokyo **15**(Suppl. 1), 78–99 (1983).
20. S. V. Patankar and D. B. Spalding, A calculation procedure for heat, mass and momentum transfer in three-dimensional parabolic flows, *Int. J. Heat Mass Transfer* **15,** 1787–1806 (1972).
21. Y. Nagano and M. Hishida, Improved form of the k–ε model for wall turbulent shear flows, *J. Fluids Engng* **109,** 156–160 (1987).